Ultrasonics 91 (2019) 220–230

Contents lists available at ScienceDirect

Ultrasonics

journal homepage: www.elsevier.com/locate/ultras

Incremental scattering of the A_0 Lamb wave mode from a notch emanating from a through-hole

Hongye Liu[a,b,c], Xin Chen[b], Jennifer E. Michaels[b,*], Thomas E. Michaels[b], Cunfu He[c]

[a] School of Optical-Electrical and Computer Engineering, University of Shanghai for Science and Technology, Jungong Road 580, Shanghai 200093, PR China
[b] School of Electrical and Computer Engineering, Georgia Institute of Technology, Atlanta, GA 30332-0250, USA
[c] College of Mechanical Engineering and Applied Electronics Technology, Beijing University of Technology, Pingleyuan 100, Chaoyang District, Beijing 100124, PR China

ARTICLE INFO

Keywords:
Lamb wave
Scattering
Finite element modeling
Laser vibrometry

ABSTRACT

Lamb wave scattering from a crack originating at a through-hole is of practical importance because of the abundance of fastener holes used in engineering structures. Notches are often used to simulate cracks so that Lamb wave methods can be more conveniently investigated in the laboratory. A linear, three-dimensional finite element model is employed in this paper to study incremental scattering of the fundamental anti-symmetric (A_0) Lamb wave mode from notches emanating from through-holes. The term "incremental scattering" refers to the change in scattering caused by introduction of the notch and is motivated by structural health monitoring for which transducers are fixed and signal changes are interpreted to detect damage. Far-field angular scattering patterns are generated for multiple incident angles and frequencies, and such patterns are experimentally validated at one frequency by laser vibrometry measurements. Comparisons are made between a vertical notch alone (no hole) and notches located above and below the through-hole. Additionally, holes of different sizes are considered to investigate the effect of hole diameter on incremental scattering patterns. Results show that the presence, location and size of the through-hole affect both the shape and strength of notch incremental scattering patterns.

1. Introduction

Lamb waves are considered to be a promising tool for non-destructive testing (NDT) and structural health monitoring (SHM) of plate-like structures [1,2]. It has been shown that Lamb waves have reasonable sensitivity to defects of interest; however, there are unavoidable issues with signal complexity. One major complexity of Lamb wave signals results from their interaction with structural features such as fastener holes. As Lamb waves travel in the structure under test, scattering occurs when they encounter both structural discontinuities and damage. Such scattering information serves as the basis for many guided wave NDT and SHM methods.

Defect scattering behavior can be described by several approaches including transmission and reflection coefficients [3], angular scattering patterns [4], and scattering matrices [5]. Transmission and reflection coefficients are usually defined as the ratio of the amplitude or energy of transmitted and reflected waves to that of the incident wave. These coefficients describe direct forward scattering and backscattering for a particular incident direction, but do not provide information about scattering at other angles. This limitation is addressed by angular scattering patterns and scattering matrices, where the former describes the 360° dependence of the amplitude of the scattered wave for a given incident direction and the latter quantifies scattering amplitudes as a function of all incident and scattered angles. Angular scattering patterns are essentially a subset of the scattering matrix. Using these approaches, the scattering of Lamb waves with several different types of scatterers can be more comprehensively investigated.

Holes are the simplest type of scatterer in engineering structures, and their effects on Lamb waves, especially the fundamental symmetric (S_0) and anti-symmetric (A_0) modes because of their reduced signal complexity, have been studied analytically [4,6–9], numerically [9,10], and experimentally [8–10]. In [4], angular scattering patterns for the S_0 mode impinging upon a part-through circular hole were provided by Grahn using an exact method based upon mode expansions of wave fields. Approximate results based on Poisson/Kirchhoff plate theory were also given but were found to be valid only for low frequencies. Cegla et al. [6] replaced the Kirchhoff plate theory used in [4] with Mindlin plate theory and obtained improved results, especially at high frequencies, for the S_0 mode scattering from part-through holes. McKeon and Hinders [7] presented a model for the scattering of the S_0

* Corresponding author.
E-mail address: jemichaels@gatech.edu (J.E. Michaels).

https://doi.org/10.1016/j.ultras.2018.08.004
Received 31 July 2017; Received in revised form 6 August 2018; Accepted 10 August 2018
Available online 11 August 2018

mode from through-holes of different diameters based upon Kane-Mindlin higher order plate theory and used the angular scattering patterns to explain the scattering effects on Lamb wave tomographic reconstruction. Fromme and Sayir [8] employed both Kirchhoff and Mindlin plate theories to calculate the angular scattering patterns of the A_0 mode from a through-hole and compared the results to experimental measurements. Diligent et al. [9] studied the scattering of the S_0 mode from circular through-holes of increasing diameters using a finite element (FE) model based upon a 2-D membrane discretization; results were validated by both analytical solutions and experiments. They subsequently developed a 3-D FE model to determine reflection coefficients of the S_0 mode from a circular part-thickness hole [10].

Cracks are another common type of scatterer, and it is well-known that they cause very different scattering patterns for ultrasonic waves impinging on them from different directions. Notches are commonly used to simulate open cracks in finite element modeling (FEM) through element removal and in experiments as they are easy to fabricate. Knowledge of scattering from expected defects can be applied to obtain improved crack detection. Examples were shown in [11] and [12] of how bulk wave scattering patterns can be used to optimize transducer installation locations for time-of-flight techniques. Another example was given by Fromme and Rouge in [13], where the angular scattering patterns of the A_0 Lamb wave mode from part-through and through-thickness notches for incident waves of different directions were measured using laser vibrometry. They suggested that these scattering directivity patterns be taken into account for guided wave array design for SHM. Knowledge of crack scattering can also provide a means of characterizing cracks. Lu et al. [14] considered a 3-D FE model to investigate the reflection, transmission, and diffraction of Lamb waves from a through-thickness crack and used reflection and transmission coefficients to estimate the crack length. Lowe et al. [15,16] studied the reflection characteristics of both the A_0 and S_0 modes at surface-breaking rectangular notches of varying widths and depths in isotropic plates using time domain FE simulations. Graphs of the reflection coefficients versus notch width were found to have a periodic shape caused by interference of waves reflected from either side of the notch. Rajagopal and Lowe [17] later studied the influence of the incident direction on the scattering of the fundamental shear horizontal guided wave (SH_0) from through-thickness cracks of different lengths and observed inference patterns between the various diffracted waves in the angular responses.

Guided waves in cylindrical tubes and pipes are similar in nature to the ones in plates when the thickness-to-diameter ratio is small but with many more propagation modes. The scattering of an arbitrary incident mode from a through-wall circumferential crack in an isotropic hollow cylinder was studied analytically by Ditri [18]. Results were given for incidence of the low order axisymmetric longitudinal mode for different crack lengths and the authors suggested how their results could be used to estimate crack sizes. The reflection of the fundamental torsional T(0,1) mode in pipes from cracks and notches of varying dimensions was investigated by Demma et al. [19] and subsequently used as a guide for interpreting corrosion measurements [20]. A generalized numerical procedure based upon wave mode expansions was developed by Bai et al. [21] to study guided wave reflection and transmission from cracks of arbitrary circumferential length and radial depth in composite pipes. The numerical results confirmed the importance of wave mode and frequency selection on crack detection.

Lamb wave scattering from a crack originating at a through-hole is of particular importance because of the abundance of fastener holes used in real structures coupled with the strong propensity of cracks to form at such holes. Compared to scattering from an edge crack (i.e., a surface-breaking crack not associated with a through-hole), scattering from a crack originating at a through-hole is potentially more complicated since scattered waves from the hole and the notch can interact with each other. To the best of the authors' knowledge, no exact analytical solution has been proposed for such scattering since analytical methods are usually limited in practice to scatterers with smooth profiles; scatterers described by tight curves or curves with discontinuous derivatives are problematic. Most existing studies have relied on FEM methods and experimental measurements. Chang and Mal [22] used a global local FEM method to identify the introduction of a notch at a through-hole by examining the frequency spectra of Lamb wave reflections. Fromme and Sayir [23] employed finite difference methods (FDM) and found the presence of a notch originating at a hole significantly changed the scattered field, but presented only one case (broadside incidence of a single mode, frequency, and plate-hole-notch geometry). Masserey and Fromme [24] also investigated the scattering of combined high frequency S_0 and A_0 modes for broadside incidence on through-thickness and part-thickness cracks at a circular hole using both FDM and experiments. The maximum scattering from a small part-thickness crack was found to be in the forward direction (shadowing of the wave behind the crack) and close to the hole, while strong scattering was observed in both the forward and backward directions for large through-thickness cracks. Bhuiyan et al. [25,26] extended the combined analytical FEM approach (CAFA) method proposed in [27] to obtain single-frequency angular scattering patterns for both the S_0 and A_0 modes incident on butterfly rivet hole cracks (two identical cracks on opposite sides of the hole).

Much of the prior research on Lamb wave scattering from cracks and notches emanating from through-holes has considered the total wavefield, which includes incident waves, hole-scattered waves, and notch-scattered waves. More recently, the field of SHM has motivated the study of incremental scattering, which refers to the change in scattering when a defect is introduced [28]. If a structure is being monitored for damage using permanently mounted transducers, there is a baseline response that includes scattered signals from geometrical features such as holes and edges. One of the ways in which damage is detected and characterized utilizes baseline subtraction, which is the subtraction of a baseline signal from the current signal of interest. For example, Chen et al. [5] applied baseline subtraction to experimentally estimate scattering patterns from fastener hole cracks using a sparse transducer array. Fromme and Rouge [13] similarly applied baseline subtraction to estimate scattering patterns from edge cracks. In the works by Bhuiyan et al. [25,26], baseline subtraction is applied to model data in the frequency domain to quantify incremental scattering of both the A_0 and S_0 modes from fastener hole cracks. Scattering patterns were presented for a 1.6 mm length butterfly crack emanating from a 6.4 mm diameter through-hole in a 3.2 mm thick plate.

Building upon the experimental investigation in [28], this paper extends the research on the effects of frequency and geometry on the incremental scattering of the A_0 mode from a single notch emanating from a through-hole. In particular, the effect of center frequency, incident direction, and hole diameter are considered, and a comparison to the scattering from a notch alone is also included. The paper is organized as follows: the FEM configuration is explained in Section 2 and the laser vibrometer experiments are described in Section 3. Data processing algorithms for both the FEM and laser measurements are detailed in Section 4. FEM results are presented in Section 5 and are compared to those obtained from the laser experiment. The effects of center frequency, incident direction, and hole diameter (including no hole at all) on the scattering are additionally considered. Scattering results are compared to those from a hole alone and a notch alone in Section 6, and concluding remarks are made in Section 7.

2. Finite element modeling

A numerical study based upon a linear FE simulation of wave propagation in an isotropic solid was undertaken to investigate the scattering of Lamb waves from a notch emanating from a through-hole. The simulation was performed using ABAQUS 6.13 based upon the full 3-D model [29]. Fig. 1 shows the configuration of the simulation. A 6061-T6 aluminum plate with dimensions of 700 mm × 700 mm × 3.175 mm

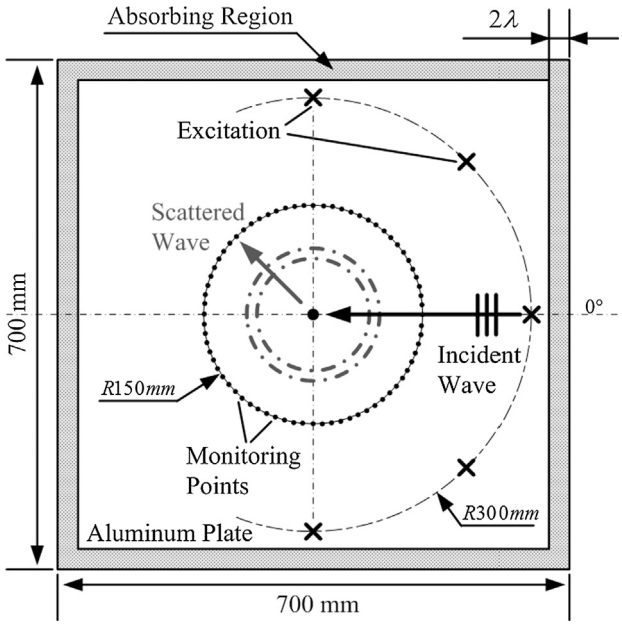

Fig. 1. Configuration for the finite element modeling.

was employed with material properties as follows: elastic modulus $E = 69$ GPa, density $\rho = 2700$ kg/m^3, and Poisson's ratio $\nu = 0.3$. Point excitation of the A_0 mode was introduced at two nodes on the top and bottom plate surfaces 300 mm from the plate center with incident directions of ± 90°, ± 135°, and 180°. The excitation pulses were 5 cycle, Hann-windowed tone bursts with center frequencies of 70 kHz, 135 kHz, and 200 kHz, resulting in nominal wavelengths of 19.5 mm, 13.1 mm, and 10.1 mm, respectively. The amplitude of the A_0 mode was monitored as the out-of-plane displacement, and monitoring points were evenly distributed around a 150 mm radius circle at 5° increments for a total of 72 points. The tone burst excitations considered here are typical of those utilized experimentally with a 3 dB bandwidth of about 30%. Although three different center frequencies are considered, results cannot be directly compared to those obtained using single frequency excitations such as were reported in [26].

Scatterers were introduced inside of a 50 mm × 50 mm region in the center of the plate by removing corresponding meshed elements. Fig. 2(a) shows a 5 mm diameter through-hole and Fig. 2(b) a vertical

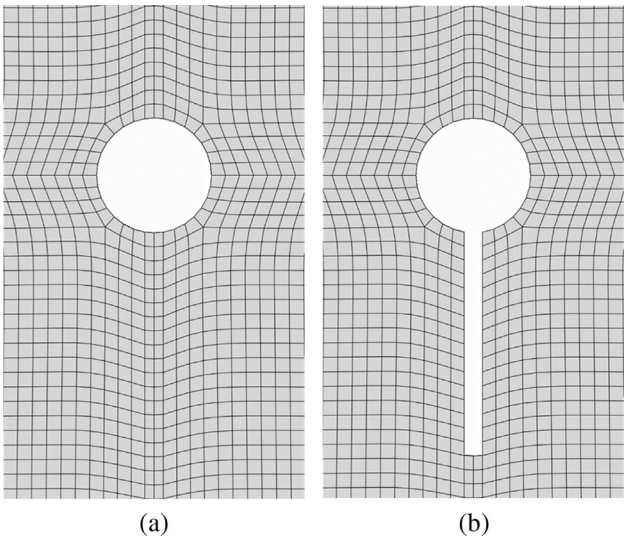

Fig. 2. Illustration of the FEM meshes in the vicinity of the scatterers. (a) The hole alone, and (b) a notch located below the hole.

10 mm notch located below (and emanating from) the hole. For these two cases, simulations were performed at all three frequencies (70, 135 and 200 kHz). Additional simulations were performed at 135 kHz for the cases of a 10 mm vertical notch alone, the notch located below (and emanating from) a 5 mm through-hole, and the notch located above (and emanating from) through-holes of five diameters (2.6, 5, 7.8, 10.4, and 13 mm). The five diameters were selected to achieve ratios of hole diameter (d) to A_0 wavelength (λ) of approximately 0.2–1 with an increment of 0.2.

To minimize boundary reflections and reduce computational requirements, absorbing regions were added at the edges of the aluminum plate by using materials with increasing damping coefficients. The width of the absorbing regions was set to twice the maximum possible wavelength of the selected excitation, which was calculated using the phase velocity of the lowest frequency component of the excitation. As a result, the amplitudes of boundary reflections should be less than 5% of that of the incident wave. The design of the absorbing regions was based on both prior literature [30,31] and experience of the authors.

Stress free boundary conditions were assumed for all the surfaces of the aluminum plate. Explicit time marching was used and the maximum time-step limit was selected as $0.8L/c$, where L is the element length and c is the largest possible wave speed, to ensure stability of the explicit marching scheme [30]. Here, a fixed time-step of 0.05 μs was used that does not exceed this limit for any of the excitation frequencies. For the spatial discretization, the meshes were designed with brick elements of length 0.625 mm, which ensures a minimum of eight elements per wavelength for all frequencies considered. The meshes in the vicinity of the scatterers used the same linear brick elements as the rest of the plate, as can be seen in Fig. 2. This meshing method effectively avoids errors caused by incompatible nodes between different geometric elements such as would occur, for example, by using tetrahedral elements near the scatterers. Although small errors might occur in the near field due to inaccurate description of the stress concentration [32], such errors are negligible since the length of elements in the model is small enough.

Fig. 3 shows a snapshot in time of FE simulation of the A_0 mode scattering from a 10 mm notch originating at a 5 mm through-hole. For the case depicted in the figure, the notch is located below the hole, the

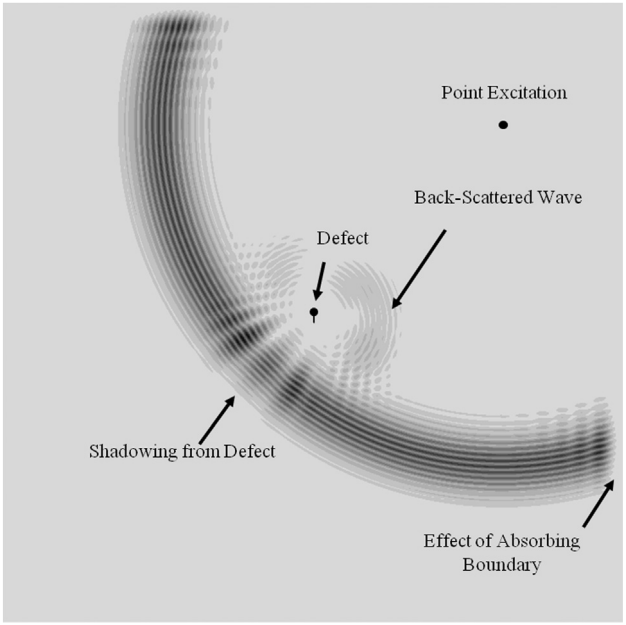

Fig. 3. Time snapshot from a typical FE simulation as viewed from the top of the plate. The excitation frequency is 135 kHz, the wavelength is 13.1 mm, the through-thickness notch length is 10 mm, the through-hole diameter is 5 mm, and the incident direction is −135°.

incident wave direction is −135°, and the excitation frequency is 135 kHz. Both the back-scattered wave and forward shadowing effects are clearly visible. No mode conversion is observed because the scatterer is symmetric about the center line of the plate thickness, and edge reflections are reasonably minimized as a result of the absorbing layers.

3. Experiments

To validate the FEM results, laser vibrometer scans were conducted using a 6061-T6 aluminum plate specimen of 1219 mm × 1219 mm × 3.175 mm with edges covered by duct sealing compound to dampen the edge reflections. The larger size of plate used in experiment compared to that in FEM is mainly to enable data collection in the far wavefield and further dampen the edge reflections. Five lead zirconate titanate (PZT) disc transducers, which are 7 mm in diameter, radially polarized, and with a resonant frequency of 300 kHz, were mounted on the plate in a semi-circular configuration separated by 45°, providing the same incident angles as those in the FE model. The radius of the array was 300 mm, which was designed to enable far-field scattering measurements while minimizing the effect of edge reflections. The transducers were excited in turn with a 50-to-500 kHz linear chirp to shorten acquisition times, reduce data storage requirements, and obtain a higher SNR [33].

The out-of-plane particle velocity was measured using a Polytec OFC-551 laser fiber vibrometer, which was controlled by a Polytec OFV-500 vibrometer controller. The vibrometer was mounted on an XYZ scanning stage that was programmed to move in a point-to-point scanning mode. A 5 mm diameter through-hole was drilled in the center of the plate followed by hand-cutting a 0.8 mm × 10 mm notch below the hole, as shown in Fig. 4. The plate remained clamped in the testing position during hole drilling and notch cutting to minimize plate repositioning errors. After each step, a full-circle laser scan was performed at a radius of 150 mm and an angular increment of 1°. The resulting laser vibrometer signals were sampled at 20 MHz, and 64 averages were applied for each acquisition to reduce incoherent noise. Each signal was digitally filtered to obtain the equivalent response to a 5-cycle, Hann-windowed tone burst excitation at 135 kHz [33].

Fig. 4. Photograph of a 10 mm hand-cut notch originating from a 5 mm diameter hole.

4. Data processing

Before extracting scattering patterns from FEM and experiments, the Lamb wave signals from the two methods need to be processed to enable valid amplitude comparisons. The first processing step is to remove the effects of different propagation distances on scattered amplitudes, resulting in scattering patterns that are only a function of incident and scattered angles. Amplitude losses are caused by both geometric spreading and dispersion, and these losses are compensated using pre-computed coefficients. The second processing step is only applied to experimental signals to compensate for excitation amplitude variations from different transducers. Multiple transducers were bonded to the specimen to excite Lamb waves from different directions, and transducer and bonding variations can cause differences in incident wave amplitudes. Such differences are compensated by comparing received signals from different transducers prior to introduction of the notch to the through-hole.

4.1. FEM data

Before extracting the scattering patterns from FEM results, the received Lamb wave signals are scaled to compensate for wave packet spreading loss (WPSL), which refers to the dispersion-caused amplitude decrease of a wave packet as it spreads in time during propagation. A WPSL(t) curve, which describes the wave packet amplitude as a function of propagation time, is pre-computed using nominal dispersion curves and its inverse is subsequently applied to measured signals to scale their amplitudes to "non-dispersive" values. Let $w_{ij}(t)$ be the received signal for the ith excitation, where $i = 1, \ldots, 5$, corresponds to the five incident angles, and the jth receiving point, where $j = 1, \ldots, 72$, corresponds to the 72 scattered angles. The scaled signal, $\widetilde{w}_{ij}(t)$, is calculated as,

$$\widetilde{w}_{ij}(t) = \frac{w_{ij}(t)}{\mathrm{WPSL}(t)}. \tag{1}$$

Using Eq. (1), both the current signal of interest and the corresponding baseline are scaled to their non-dispersed amplitudes, $\widetilde{w}_{ij}(t)$ and $\widetilde{w}^{b}_{ij}(t)$, respectively. The residual signal, $u_{ij}(t)$, is obtained by baseline subtraction as:

$$u_{ij}(t) = \widetilde{w}_{ij}(t) - \widetilde{w}^{b}_{ij}(t), \tag{2}$$

The envelope-detected residual signal, $r_{ij}(t)$, is calculated using the Hilbert transform (denoted by $\mathscr{H}[\cdot]$),

$$r_{ij}(t) = |u_{ij}(t) + i\mathscr{H}[u_{ij}(t)]|. \tag{3}$$

The scattered amplitude, R_{ij}, is obtained from the peak of the directly scattered wave packet of $r_{ij}(t)$. The scattering coefficient, S_{ij}, is calculated by dividing the scattered amplitude by that of the incident wave, where both are adjusted to their values at the scatterer location (taken here to be the mid-point of the notch) with appropriate compensation for geometric spreading loss (GSL),

$$S_{ij} = \frac{R_{ij}\sqrt{D_{sj}}}{I_{ij}}, \quad \text{where} \quad I_{ij} = \frac{A_{ij}\sqrt{D_{ij}}}{\sqrt{D_{is}}}. \tag{4}$$

Here, D_{sj} is the distance from the scatterer s to the receiving point j, A_{ij} is the amplitude of the direct arrival of the baseline signal, D_{ij} is the distance between the excitation and receiving points, and D_{is} is the distance between the excitation point and the scatterer. Note that D_{sj} can be slightly different than the nominal distance of 150 mm because of the discrete mesh of the FE simulation.

4.2. Laser measurements

Different than the FE simulation, which uses the same signal for all excitations, the laser records signals generated by different bonded

transducers, each of which corresponds to a different incident direction. Therefore, in additional to the WPSL and GSL compensations for each measured signal, the laser measurements need to be compensated for transducer and bonding variations. Appropriate scale factors for each transducer are determined by analyzing laser data that are acquired from the hole alone prior to introduction of the notch. Data from each transducer should be nominally identical after an appropriate rotation to the same incident direction; readers are referred to [5] for a more complete description. The same scaling coefficients are also used to compensate the hole-plus-notch signals. The scattering coefficients are then obtained using the same procedures employed for the FE data, including WPSL compensation, baseline subtraction, and GSL compensation.

5. Results

In this section, typical signals from one FE simulation are first shown. Then, angular scattering patterns from the FE simulation are validated by laser measurements. After validation, FEM results are shown to illustrate the effects of frequency, notch position, and hole diameter on scattering patterns.

5.1. FEM example signals

Fig. 5 shows scaled scattered signals for two FEM monitoring nodes for the 10 mm notch located below the 5 mm diameter hole. The A_0 Lamb wave mode with a center frequency of 135 kHz is incident at a propagation direction of 180°. Fig. 5(a) shows the signals for a scattering direction of 180°, where the hole signal (baseline) is plotted with a gray line and the hole-plus-notch signal with a black line. Such an excitation-monitoring combination represents forward scattering, resulting in the scattered wave packet overlapping with the direct arrival. Introducing of the notch reduces the amplitude of the hole-plus-notch signal, and the residual signal is plotted with the dashed black line. Fig. 5(b) shows the +90° scattering direction case, where the scattered wave packet is distinctly separated from the direct arrival. The scattering amplitude is smaller than that for a scattering angle of 180° case, demonstrating the strong angular dependence of the scattering.

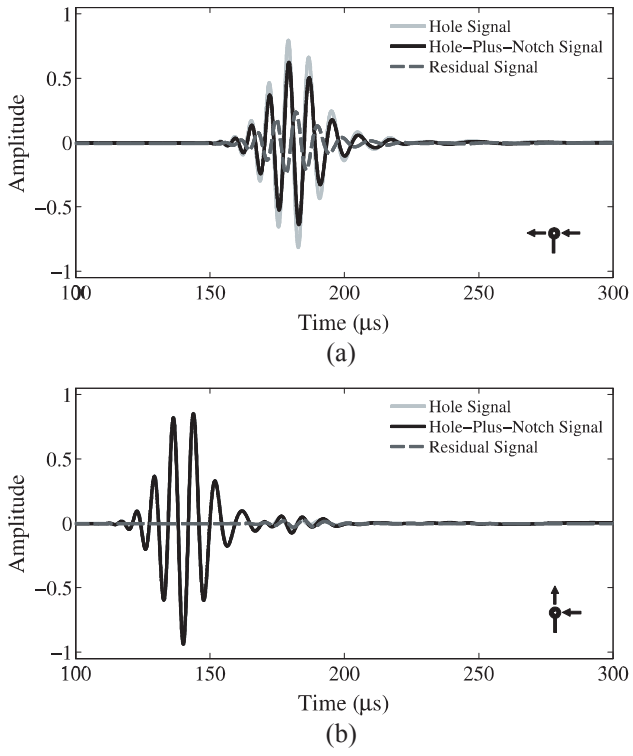

Fig. 5. Signals from the FE model received at scattered angles of (a) 180° and (b) 90°. The incident direction is 180° and the excitation frequency is 135 kHz.

5.2. Experimental validation of scattering patterns

Fig. 6 shows angular scattering patterns from the 10 mm notch located below the 5 mm diameter through-hole for an excitation frequency of 135 kHz and all five incident angles. These scattering patterns were computed relative to the center of the hole, which was also the center of the plate. The solid black line represents the FEM results and the gray "+" symbols show the laser measurements. The scattering pattern for the broadside incident wave (180°) is shown in Fig. 6(a), and there is very good agreement between the FEM and experimental scattering patterns. Two main lobes that represent strong forward and back scattering are clearly observed and almost no scattering occurs at ± 90°, both of which are consistent with the signals of Fig. 5.

Fig. 6(b) and (c) show angular scattering patterns when the incident waves are oblique to the hole-plus-notch (± 135°). Both figures indicate good agreement between the FEM results and laser measurements, despite slight amplitude differences. Comparing these two figures to Fig. 6(a), the maximum scattered amplitude occurs in Fig. 6(c), for the case where the incident wave is approaching the hole-plus-notch at an angle of −135° (the "hole" end). The smallest scattered amplitude is in Fig. 6(b) for an incident direction of + 135° (the "notch" end), and the broadside direction is in-between. Both the scattering patterns in Fig. 6(b) and (c) also show more structure as compared to Fig. 6(a); i.e., four lobes rather than two. These two patterns are not mirror images about the *x*-axis, which would be the case for a notch alone. Even though the scattering patterns are incremental (i.e., change in scattering caused by the notch), the presence of the hole definitely affects the scattering behavior.

The effect of the hole can be further observed in Fig. 6(d) and (e), where Lamb waves are incident from the end-on directions (± 90°). As expected, the overall scattering amplitudes are much smaller compared to broadside incidence (note the different amplitude scales). The forward scattered laser measurements are very noisy because of the difficulty in separating the small forward scattered signals from the much stronger direct arrivals. Nevertheless, the FEM results still agree reasonably well with the laser measurements both in the shape of the patterns and their amplitudes. For both of these two incident angles, the scattering patterns obtained from FEM are symmetric about the notch orientation (the *y*-axis) because of the geometric symmetry of the scatter. However, this is not the case for the laser measurements, which can be attributed to both imperfect manual cutting of the notch and the very noisy forward-scattered results. The marked differences in these two end-on scattering patterns can best be seen in the FEM results, and again indicate that the presence of the hole strongly influences the scattering behavior.

5.3. Frequency dependence of scattering patterns

Fig. 7 shows angular scattering patterns computed relative to the hole center for three different center frequencies (70, 135, and 200 kHz), again for the introduction of the 10 mm notch below the 5 mm through-hole. Recall that the corresponding wavelengths are 19.5, 13.1, and 10.1 mm, so as the frequency increases from 70 to 200 kHz, the wavelength decreases from about twice the notch length to essentially the same as the notch length. The patterns for the three frequencies are shown by solid gray lines for 70 kHz, dashed black lines for 135 kHz, and solid black lines for 200 kHz. For the broadside incidence case of Fig. 7(a), two main lobes are observed for all three frequencies. The effects of frequency are small, although the medium frequency, 135 kHz, has slightly smaller forward scattering amplitudes than those of the other two frequencies.

Fig. 7(b) and (c) show the angular scattering patterns for incident

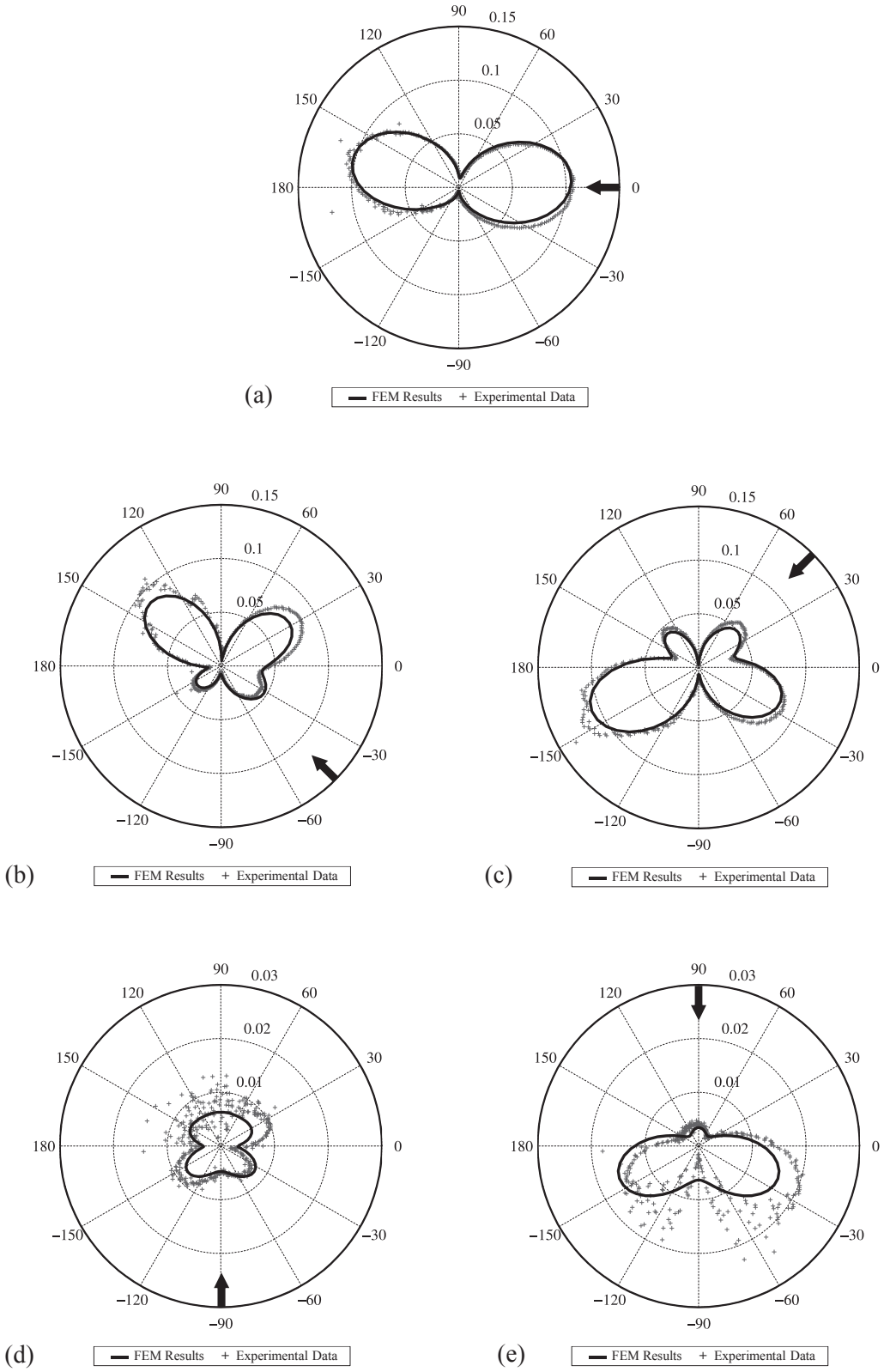

Fig. 6. Simulated and measured angular scattering patterns at 135 kHz from a 10 mm vertical notch located below a 5 mm diameter through-hole for incident directions of (a) 0°, (b) +135°, (c) −135°, (d) +90°, and (e) −90°. The black arrows indicate the incident directions.

angles of +135° and −135°, respectively. Both patterns show that as the frequency increases (i.e., as the wavelength decreases and approaches the notch length), more lobe structure is observed. In particular, there is an obvious change from a two-lobed scattering pattern similar to broadside incidence at 70 kHz to a four-lobed pattern at 135 and 200 kHz. Another observation is that the scattering becomes stronger for all lobe regions, especially the forward scattering region, as the frequency increases and the wavelength approaches the notch length, which is as expected.

Similar observations can also be made for Fig. 7(d) and (e), which

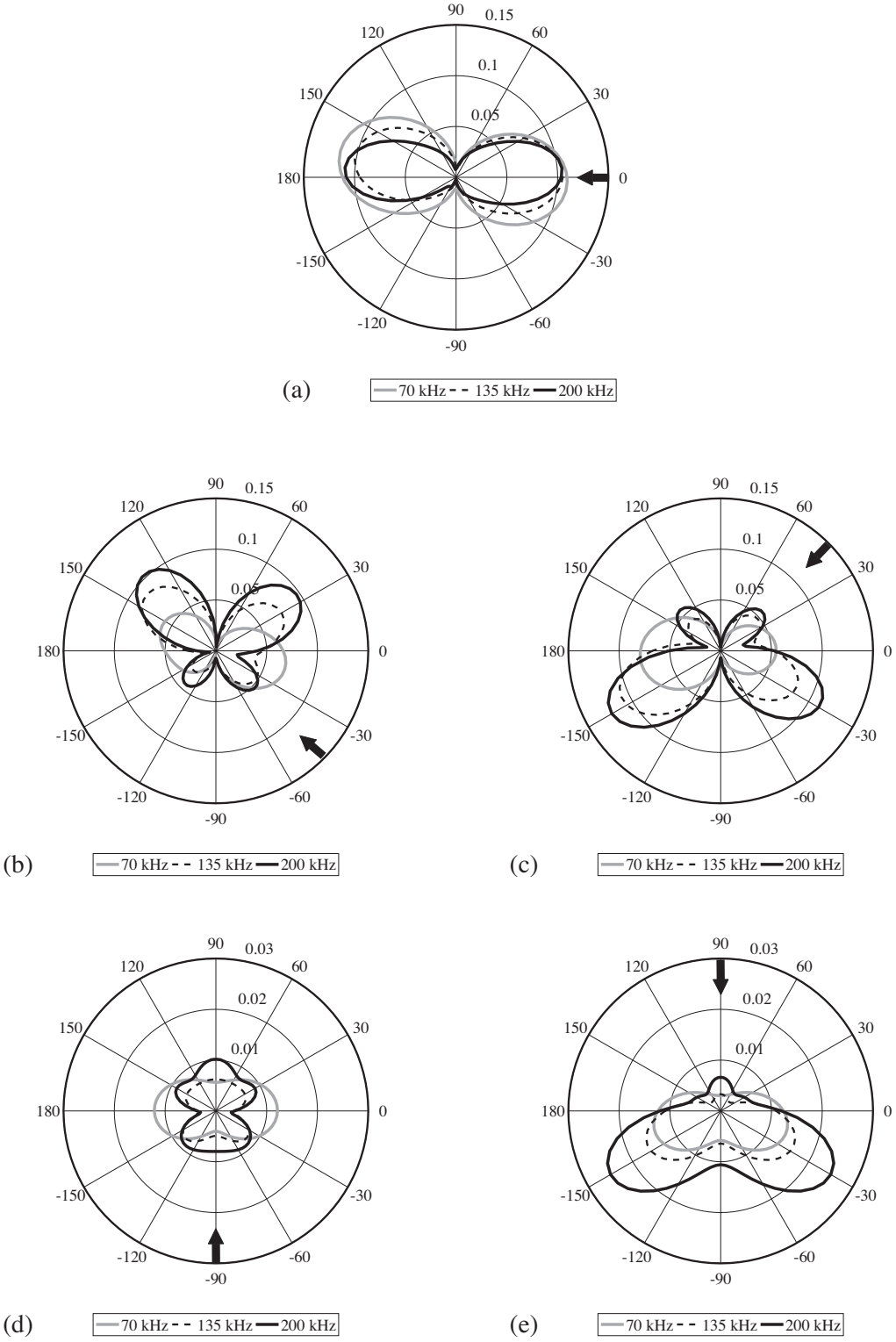

Fig. 7. Simulated angular scattering patterns for three different excitation frequencies from a 10 mm vertical notch located below a 5 mm diameter through-hole for incident directions of (a) 180°, (b) +135°, (c) −135°, (d) +90°, and (e) −90°. The black arrows indicate the incident directions.

show the incremental scattering patterns for end-on incidence (± 90°). Note that the amplitude scale for these two plots is one-fifth of the scale for the other three, which highlights the overall much weaker scattering for end-on incidence. For Fig. 7(d), the wave impinges upon the notch first, whereas for Fig. 7(e), the wave impinges upon the hole first. For all three frequencies, the overall incremental scattering is stronger for the case where the wave impinges upon the hole first, and the differences in both scattering strength and shape increase with frequency. The width of the notch is much smaller than the wavelength for all three frequencies, so the waves approaching the notch tip are not strongly affected by it. Most of the notch scattering likely arises from waves being guided around the hole circumference and then interacting with the much larger notch faces. For the case of +90° impingement (wave hits the notch tip first), the incident wave must complete a full

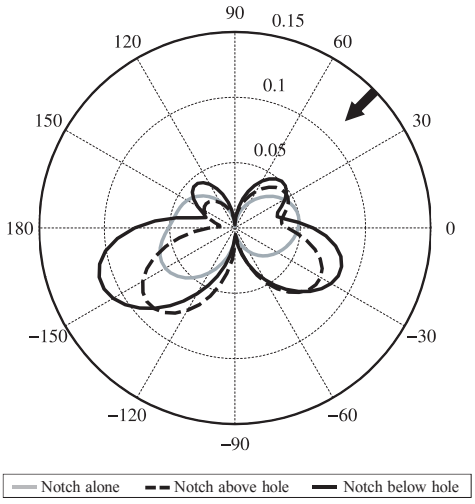

(a)

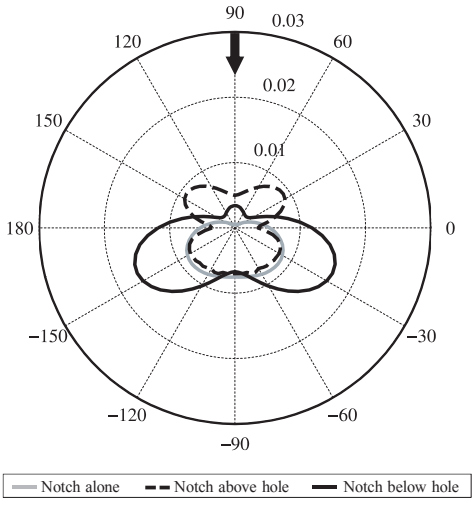

(b)

Fig. 8. Simulated angular scattering patterns at 135 kHz from a 10 mm notch alone, from the notch above a 5 mm diameter through-hole, and from the notch below the through-hole. Incident directions are (a) −135° and (b) −90°. The black arrows indicate the incident directions.

traverse around the hole before interacting with the notch faces, whereas for the −90° case (wave hits the hole first), only half of a revolution is required, leading to larger scattering amplitudes.

5.4. Influence of notch position on scattering patterns

The plots of Fig. 7 provide some insight on the effect of the notch position relative to the incident wave direction on the scattering patterns. Fig. 8 provides a more direct comparison for incident directions of −135° and −90° at a frequency of 135 kHz by also considering a notch alone. The notch length is 10 mm and the hole diameter is 5 mm. These patterns were generated relative to the center of the notch rather than the center of the hole and are thus slightly different than the corresponding ones in Fig. 7 (for the cases with the hole). The patterns for the three cases are shown by solid gray lines for the notch alone, dashed black lines for the notch above the hole, and solid black lines for the notch below the hole. For an incident direction of −135° as shown in Fig. 8(a), the patterns for the three cases are distinctly different. The notch-only pattern has only two lobes whereas both hole-plus-notch patterns have four lobes. The maximum amplitudes are also different with the smallest amplitude for the notch alone and the largest for notch below the hole. Comparing the shapes of the patterns for the two hole-plus-notch cases, the most obvious difference is the directionality of the two largest lobes. For the notch above the hole, the peak of the forward scattered lobe is almost directly in-line with the incident wave. The other large lobe is at an angle of approximately −45°, as if it were a specular reflection from a vertical edge. For the notch below the hole, the directions of these two lobes are bent towards 180° and 0° by at least 20°. Interestingly, the scattering from the notch alone shows no evidence of a separate lobe near −45° with both the forward scattering and backscattering lobes tipped away from the horizontal toward the incident wave direction.

Fig. 8(b) further shows the effects of the notch position on scattering for an incident direction of −90°. Similar to Fig. 8(a), the notch-only pattern has the smallest amplitudes overall and the notch below the hole has the largest. All three patterns have very similar forward scattered amplitudes at −90°, directly opposite the incident direction, even though the patterns are quite different. Both of the hole-plus-notch cases have more lobe structure as compared to the notch alone. The forward scattering pattern for the notch above the hole is almost identical to that of the notch alone, whereas the backscattering is much stronger. The forward scattering for the notch below the hole is quite different from the other two cases with much larger side-scattered lobes, while the backscattering shows a small local peak at +90°.

5.5. Influence of hole diameter on scattering patterns

Fig. 9 shows the effect of hole diameter on scattering patterns for the 135 kHz excitation, an incident direction of −135°, and the notch located above the hole. The notch length is 10 mm and the five hole diameters considered are 2.6 mm ($d/\lambda \approx 0.2$), 5 mm ($d/\lambda \approx 0.4$), 7.8 mm ($d/\lambda \approx 0.6$), 10.4 mm ($d/\lambda \approx 0.8$), and 13 mm ($d/\lambda \approx 1.0$), where d/λ is the ratio of hole diameter to wavelength. Note that these patterns were computed relative to the center of the notch, not the hole. Even for the smallest hole diameter, there are clearly four lobes as compared to the two-lobed structure for the notch alone. The scattering patterns remain similar until the hole diameter is about the same as the notch length, although there are small changes in lobe amplitudes and directions. As the hole diameter increases further, the largest forward scattering values start to decrease and the scattering patterns also change such that there is more structure within the forward scattering lobe (i.e., amplitude fluctuations within the lobe). These changes are not strictly monotonic with hole size, and are likely due to interference effects as the notch-scattered waves travel around the various diameter holes.

To further illustrate incremental scattering changes as a result of $d/$

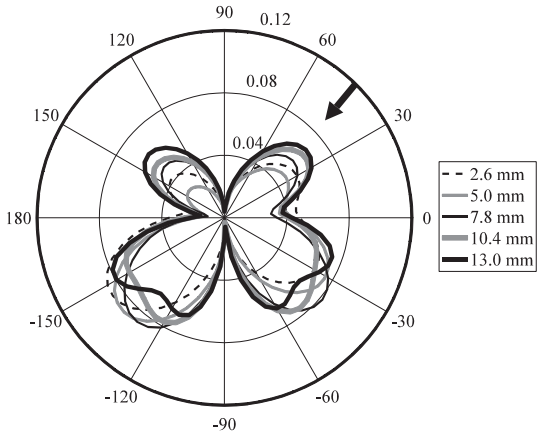

Fig. 9. Simulated angular scattering patterns at 135 kHz from a 10 mm vertical notch located above through-holes of five different diameters for an incident direction of −135°. The black arrow indicates the incident direction.

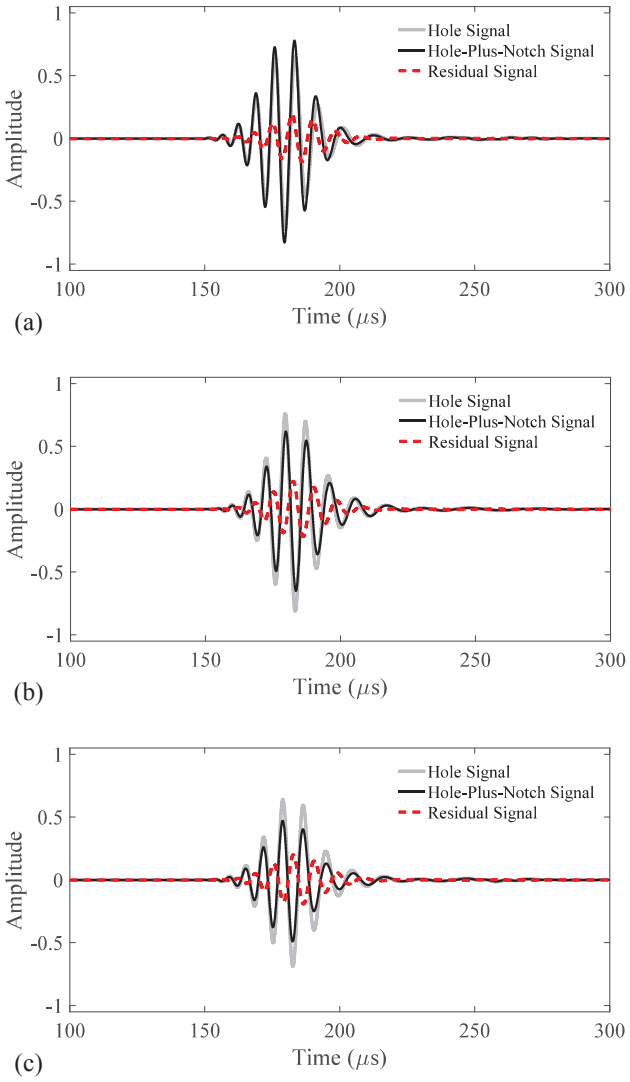

Fig. 10. Signals from the FE model received at scattered angles of (a) −115°, (b) −130°, and −140°. The scatterer is a 10 mm vertical notch located above a 7.8 mm diameter hole. The incident direction is −135° and the excitation frequency is 135 kHz.

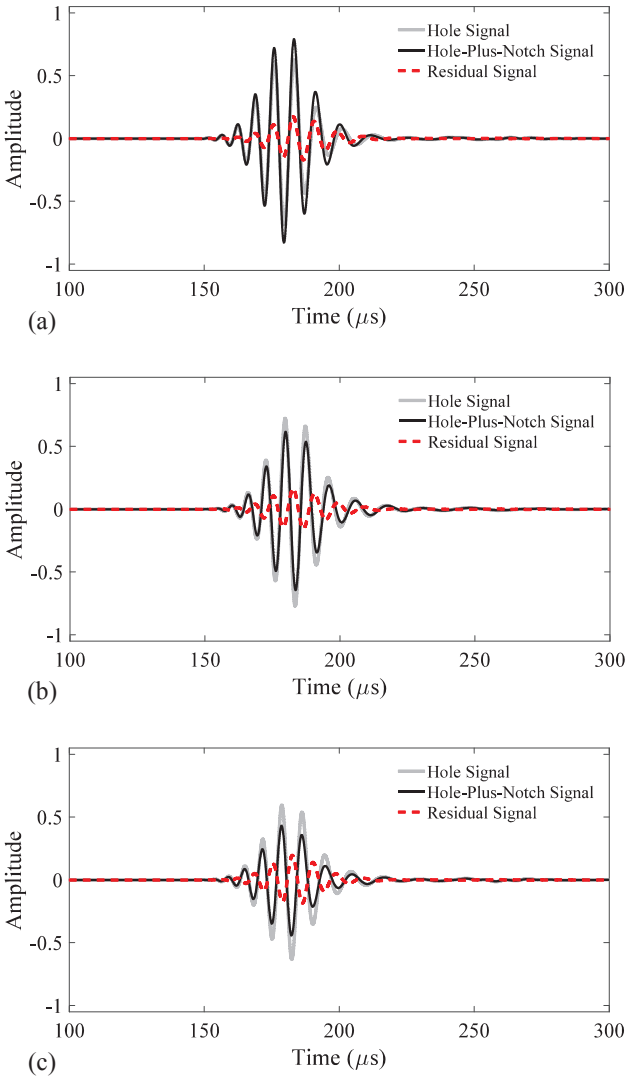

Fig. 11. Signals from the FE model received at scattered angles of (a) −115°, (b) −130°, and −140°. The scatterer is a 10 mm vertical notch located above a 13.0 mm diameter hole. The incident direction is −135° and the excitation frequency is 135 kHz.

λ ratio, time-domain signals are shown for hole diameters of 7.8 mm and 13.0 mm in Figs. 10 and 11, respectively, at the three scattered angles of −115°, −130°, and −145°. These angles correspond to the shadow region on the far side of the hole (relative to the incident wave) and signal changes thus indicate the effect of the hole and the combined hole-plus-notch on the transmitted wave. For both figures, the hole signal (baseline) is plotted with a gray line, the hole-plus-notch signal with a black line, and the residual signal with a dashed line.

Both figures show very similar decreasing amplitude trends for the hole signals and the hole-plus-notch signals as the scattered angle changes from −115° to −130° to −145°. An examination of the residual signals indicates that there are also small phase changes that affect the amplitudes of the residuals. In Fig. 10 for the 7.8 mm diameter hole, the net result is a peak in the residual signal amplitude at −130° whereas in Fig. 11 for the 13.0 mm diameter hole there is a local minimum. These differences are manifested as distinctly different shapes in the forward scattered lobes in Fig. 9, which further supports the idea of the hole causing interference effects in the notch-scattered waves.

6. Discussion

The incremental scattering results shown here for the hole-plus-notch can be better understood in the context of prior scattering results for through-holes alone and notches alone. For a through-hole, angular scattering patterns of the A_0 mode have a simple two-lobed structure for wavelengths much larger than the hole diameter (small d/λ ratio) with similar backscattered and forward-scattered amplitudes [34]. There are few if any reported results for higher frequencies, but it is expected that scattering patterns would become more complicated due to interference of the incident and scattered waves as reported for the S_0 mode [4,6] and for bulk shear waves polarized parallel to a cylindrical hole [35]. This general behavior can also be observed for the A_0 mode by examining the total field results reported in [8]. Regardless of the d/λ ratio, the axisymmetric geometry leads to scattering patterns that are symmetric about the incident direction.

The situation is different for scattering from a notch alone [13,36]. For the low frequency case where the wavelength is larger than twice the notch length, the scattering pattern is quite simple but with backscattering being much less than shadowing of the incident wave by the notch. The forward and backscattered lobes are almost exactly aligned with the normal to the notch even for waves approaching the notch

obliquely. As the wavelength decreases to the notch length, the simple two-lobed pattern aligned with the notch normal is maintained for incident directions close to the notch normal, but splits into a four-lobed pattern as the incident direction approaches -135°. Very little scattering is observed for end-on incident angles. As expected from reciprocity, there is also very little scattering for the same end-on scattered angles regardless of the incident direction.

For the results shown here for the hole-plus-notch, the wavelength varies from two to four times the 5 mm hole diameter for the three frequencies considered, and from one to two times the 10 mm notch length. The scattering results of Fig. 7 qualitatively agree with those reported in [13] and [36] from the notch alone in that for $\pm 135^{\circ}$ incidence there is a two-lobed pattern roughly aligned with the notch normal for low frequencies that changes to a four-lobed pattern at higher frequencies. The asymmetrical presence of the hole causes the $+135^{\circ}$ and -135° patterns to be somewhat different but does not change the four-lobed structure. A comparison to the notch alone in Fig. 8(a) at 135 kHz indicates that the presence of the hole causes the transition from two to four lobes to occur at a lower frequency than it would otherwise. The presence of the hole increases the d/λ ratio from below one (0.76 for the notch only) to above one (1.15 for the hole-plus-notch), and the complexity of the scattering pattern increases as would be expected. For the patterns shown in Fig. 9 for different hole diameters, the four-lobed structure is present for all cases. This result is not surprising since the d/λ ratio for the combined scatterer varies from 0.96 for the hole diameter of 2.6 mm to 1.76 for the 13.0 mm hole diameter; the scatterer is never small enough compared to the wavelength to achieve the simple two-lobed scattering pattern.

7. Summary and conclusions

The incremental scattering of the A_0 Lamb wave mode from a vertical notch ($\ell = 10$ mm) emanating from a hole in a 3.175 mm thick aluminum plate was investigated by both FE modeling and experimental measurements. Excellent agreement was found between incremental scattering patterns determined by both simulation and experiment. Both techniques show that the scattering patterns are asymmetric about the normal to the notch, slightly so for broadside incidence and becoming increasingly asymmetric as the incident directions become parallel to the notch.

The FE modeling was further used to study the effect of excitation frequency on the incremental scattering patterns. As expected, the patterns have more lobe structure as the frequency increases, transitioning from a relatively simple two-lobed structure at $\lambda = 2\ell$ for all incident angles considered to more complicated patterns at higher frequencies ($\lambda = 1.3\ell$ and $\lambda = \ell$). For oblique incidence at the higher frequencies considered, there is a distinctive four-lobed structure regardless of whether the notch is located above or below the hole. The effect of hole diameter was investigated at one frequency ($\lambda = 1.3\ell$). It was shown that the scattering patterns retain a four-lobed structure even for the smallest diameter considered whereas the simpler two-lobed structure is observed for the notch alone. The presence of the hole was found to significantly complicate incremental scattering patterns because the hole itself can enable additional scattering of notch-scattered waves and the scattering patterns incorporate the effect of the notch on hole-scattered waves. The presented results show that the basic scattering patterns are similar to those for a notch alone but the presence of the hole increases the overall dimensions of the scatterer and causes a transition to more complicated scattering patterns at lower frequencies than would be expected from the notch alone.

These findings can serve as guidance when interpreting changes in Lamb wave signals caused by scattering from fastener hole cracks, and can further assist in the design of permanently attached transducer arrays for structural health monitoring. As prior studies with notches have shown, there are peaks and nulls in the scattering patterns whose angular locations must be taken into consideration when deploying sensors. This current work shows the importance of taking both frequency and the presence of the hole into account when considering incremental scattering patterns and not relying on results from a notch alone.

Acknowledgements

Dr. Hongye Liu was supported by the National Natural Science Foundation of China (Grant Nos. 51235001, 11372016, 51705325) and the China Scholarship Council. The experimental work was sponsored by the American Society for Nondestructive Testing (ASNT) in the form of a Graduate Fellowship to Dr. Xin Chen.

References

[1] J.L. Rose, A baseline and vision of ultrasonic guided wave inspection potential, J. Press. Vess. Technol. 124 (3) (2002) 273–282.
[2] A. Raghavan, C.E.S. Cesnik, Review of guided-wave structural health monitoring, Shock Vib. Dig. 39 (2) (2007) 91–114.
[3] Y.N. Al-Nassar, S.K. Datta, A.H. Shah, Scattering of Lamb waves by a normal rectangular strip weldment, Ultrasonics 29 (2) (1991) 125–132.
[4] T. Grahn, Lamb wave scattering from a circular partly through-thickness hole in a plate, Wave Motion 37 (1) (2003) 63–80.
[5] X. Chen, J.E. Michaels, T.E. Michaels, A methodology for estimating guided wave scattering patterns from sparse transducer array measurements, IEEE Trans. Ultrason., Ferroelectr. Freq. Control 62 (1) (2015) 208–219.
[6] F.B. Cegla, A. Rohde, M. Veidt, Analytical prediction and experimental measurement for mode conversion and scattering of plate waves at non-symmetric circular blind holes in isotropic plates, Wave Motion 45 (3) (2008) 162–177.
[7] J.C.P. McKeon, M.K. Hinders, Lamb wave scattering from a through hole, J. Sound Vib. 224 (5) (1999) 843–862.
[8] P. Fromme, M.B. Sayir, Measurement of the scattering of a Lamb wave by a through hole in a plate, J. Acoust. Soc. Am. 111 (3) (2002) 1165–1170.
[9] O. Diligent, T. Grahn, A. Boström, P. Cawley, M.J.S. Lowe, The low-frequency reflection and scattering of the S_0 Lamb mode from a circular through-thickness hole in a plate: finite element, analytical and experimental studies, J. Acoust. Soc. Am. 112 (6) (2002) 2589–2601.
[10] O. Diligent, M.J.S. Lowe, Reflection of the S_0 Lamb mode from a flat bottom circular hole, J. Acoust. Soc. Am. 118 (5) (2005) 2869–2879.
[11] J.A. Ogilvy, J.A.G. Temple, Diffraction of elastic waves by cracks: application to time-of-flight inspection, Ultrasonics 21 (1983) 259–269.
[12] C.B. Scruby, K.R. Jones, L. Antoniazzi, Diffraction of elastic waves by defects in plates: calculated arrival strengths for point force and thermoelastic sources of ultrasound, J. Nondestruct. Eval. 5 (3–4) (1986) 145–156.
[13] P. Fromme, C. Rouge, Directivity of guided ultrasonic wave scattering at notches and cracks, J. Phys.: Conf. Ser. 269 (2011) 11 no. 012018.
[14] Y. Lu, L. Ye, Z. Su, C. Yang, Quantitative assessment of through-thickness crack size based on Lamb wave scattering in aluminum plates, NDT & E Int. 41 (1) (2008) 59–68.
[15] M.J.S. Lowe, O. Diligent, Low-frequency reflection characteristics of the S_0 Lamb wave from a rectangular notch in a plate, J. Acoust. Soc. Am. 111 (1) (2002) 64–74.
[16] M.J.S. Lowe, P. Cawley, J.Y. Kao, O. Diligent, The low frequency reflection characteristics of the fundamental antisymmetric Lamb wave a_0 from a rectangular notch in a plate, J. Acoust. Soc. Am. 112 (6) (2002) 2612–2622.
[17] P. Rajagopal, M.J.S. Lowe, Angular influence on scattering when the fundamental shear horizontal guided wave mode is incident at a through-thickness crack in an isotropic plate, J. Acoust. Soc. Am. 124 (5) (2008) 2021–2030.
[18] J.J. Ditri, Utilization of guided elastic waves for the characterization of circumferential cracks in hollow cylinders, J. Acoust. Soc. Am. 96 (6) (1994) 3769–3775.
[19] A. Demma, P. Cawley, M. Lowe, A.G. Roosenbrand, The reflection of the fundamental torsional mode from cracks and notches in pipes, J. Acoust. Soc. Am. 114 (2) (2003) 611–625.
[20] A. Demma, P. Cawley, M. Lowe, A.G. Roosenbrand, B. Pavlakovic, The reflection of guided waves from notches in pipes: a guide for interpreting corrosion measurements, NDT & E Int. 37 (3) (2004) 167–180.
[21] H. Bai, A.H. Shah, N. Popplewell, S.K. Datta, Scattering of guided waves by circumferential cracks in composite cylinders, Int. J. Solids Struct. 39 (17) (2002) 4583–4603.
[22] Z. Chang, A. Mal, Scattering of Lamb waves from a rivet hole with edge cracks, Mech. Mater. 31 (3) (1999) 197–204.
[23] P. Fromme, M.B. Sayir, Detection of cracks in rivet holes using guided waves, Ultrasonics 40 (1) (2002) 199–203.
[24] B. Masserey, P. Fromme, Analysis of high frequency guided wave scattering at a fastener hole with a view to fatigue crack detection, Ultrasonics 76 (2017) 78–86.
[25] M.Y. Bhuiyan, Y. Shen, V. Giurgiutiu, Guided wave based crack detection in the rivet hole using global analytical with local FEM approach, Materials 9 (7) (2016) 602.
[26] M.Y. Bhuiyan, Y. Shen, V. Giurgiutiu, Interaction of Lamb waves with rivet hole cracks from multiple directions, Proc. Inst. Mech. Eng., Part C: J. Mech. Eng. Sci. 231 (16) (2017) 2974–2987.

[27] Y. Shen, V. Giurgiutiu, Combined analytical FEM approach for efficient simulation of Lamb wave damage detection, Ultrasonics 69 (2016) 116–128.
[28] X. Chen, J.E. Michaels, T.E. Michaels, Incremental scattering of guided waves from a notch originating at a through-hole, Rev. Prog. Quant. Nondest. Eval., AIP Conf. Proc. 1650 (2015) 799–806.
[29] Abaqus Analysis User's Guide, v6.13, Dassault Systems, 2013 (www.3ds.com).
[30] M.J.S. Lowe, D.N. Alleyne, P. Cawley, The mode conversion of a guided wave by a part-circumferential notch in a pipe, J. Appl. Mech. 65 (3) (1998) 649–656.
[31] L. Moreau, M. Castaings, The use of an orthogonality relation for reducing the size of finite element models for 3D guided waves scattering problems, Ultrasonics 48 (5) (2008) 357–366.
[32] P. Fromme, Influence of guided ultrasonic wave scattering directionality on the detection sensitivity for SHM of fatigue cracks, *Proceedings of the SPIE* **7650**, paper no. 76501M, 2010.
[33] J.E. Michaels, S.J. Lee, A.J. Croxford, P.D. Wilcox, Chirp excitation of ultrasonic guided waves, Ultrasonics 53 (1) (2013) 265–270.
[34] M.B. Obenchain, C.E. Cesnik, Guided wave interaction with hole damage using the local interaction simulation approach, Smart Mater. Struct. 23 (2014) 125010.
[35] K.F. Graff, Wave Motion in Elastic Solids, Dover Publications, New York, 1975.
[36] P. Fromme, Structural health monitoring of stiffened plates using guided ultrasonic waves, Rev. Prog. Quant. Nondest. Eval., AIP Conf. Proc. 1096 (2009) 998–1005.